

# Normalizing kernels in the Billera-Holmes-Vogtmann treespace

Grady Weyenberg

Daniel K Howe

Ruriko Yoshida

## Abstract

**Motivation:** As costs of genome sequencing have dropped precipitously, development of efficient bioinformatic methods to analyze genome structure and evolution have become ever more urgent. For example, most published phylogenomic studies involve either massive concatenation of sequences, or informal comparisons of phylogenies inferred on a small subset of orthologous genes, neither of which provides a comprehensive overview of evolution or systematic identification of genes with unusual and interesting evolution (e.g. horizontal gene transfers, gene duplication and subsequent neofunctionalization). We are interested in identifying such “outlying” gene trees from the set of gene trees and estimating the distribution of the tree over the “tree space”.

**Results:** This paper describes an improvement to the KDETREES algorithm, an adaptation of classical kernel density estimation to the metric space of phylogenetic trees (Billera-Holmes-Vogtmann treespace), whereby the kernel normalizing constants, are estimated through the use of the novel holonomic gradient methods. As the original `kdetrees` paper, we have applied `kdetrees` to a set of Apicomplexa genes and it identified several unreliable sequence alignments which had escaped previous detection, as well as a gene independently reported as a possible case of horizontal gene transfer.

**Availability:** The updated version of the KDETREES software package is available both from CRAN (the official R package system), as well as from the official development repository on Github. ([github.com/grady/kdetrees](https://github.com/grady/kdetrees)).

**Contact:** [ruriko.yoshida@uky.edu](mailto:ruriko.yoshida@uky.edu)

## 1 Introduction

One of the great opportunities offered by modern genomics is that phylogenetics applied on a genomic scale (phylogenomics) should be especially powerful for elucidating gene and genome evolution, relationships among species and populations, and processes of speciation and molecular evolution. However, a well-recognized hurdle is the sheer volume of genomic data that can now be generated relatively cheaply and quickly, but for which analytical tools are lagging. There is a major need to explore new approaches to undertake comparative genomic and phylogenomic studies much more rapidly and robustly than existing tools allow. Here, we focus on the problem of *efficiently* identifying significant *discordance* among a set of gene trees, as well as estimating the distribution of gene trees from the given set of trees.

The KDETREES algorithm introduced in Weyenberg *et al.* [2014] is an adaptation of classical kernel density estimation to the metric space of phylogenetic trees defined by Billera *et al.* [2001]. It is a computationally efficient method of estimating the density of the trees over the Billera-Holmes-Vogtmann (BHV) treespace, and relies on a fast implementation of the BHV geodesic distance function provided by Owen and Provan [2011]. The method then uses the density estimates to identify putative outlier observations. This paper describes an improvement to KDETREES, whereby the kernel normalizing constants, are estimated through the use of the novel holonomic gradient methods [Koyama *et al.*, 2014; Marumo *et al.*, 2014].

In our original paper describing the KDE TREES method, we propose a nonparametric estimator of the form,

$$\hat{f}(T) \propto \frac{1}{N} \sum_{i=1}^N k(T, T_i, h_i).$$

In the KDE TREES software, the kernel function implemented is a spherically symmetric gaussian kernel, i.e.

$$k(T, T', h) \propto \exp\left(-\left(\frac{d(T, T')}{h}\right)^2\right). \quad (1)$$

Since we are, for the moment, interested primarily in using the estimator  $\hat{f}$  for outlier detection, knowledge of the overall proportionality constant for  $\hat{f}$  is not of significant importance. However, it is important to know how the normalizing constant associated with  $k(T, T', h)$  varies with the selected bandwidth and with the location of the kernel's center. In our original paper we argued that, in practice, estimates of the normalizing constant do not appear to have significant systematic variation, and that assuming a constant value was a reasonable first approximation. This paper presents basic results and techniques for obtaining better approximate values for these normalizing constants.

In the case of Euclidean  $k$ -space with the usual metric, the kernel (1) corresponds to a spherically symmetric multivariate normal distribution centered on the point  $T'$ , and the kernel normalization constant is given by

$$c(T', h_i) = (2\pi h_i)^{-k/2}. \quad (2)$$

Note that not only is there a simple closed form solution for the constant, but the constant is invariant under changes to the central point  $T'$ . However, when applied to the BHV treespace with the geodesic metric, not only is such a closed form solution apparently unavailable, but it is also clear that the constant will depend on the location of the central point.

For example, consider the case where  $T' = 0$ , i.e., the star tree, located at the origin of BHV space. In this case, the kernel integral,

$$c(T', h) = \int_{\mathcal{T}} k(T, T', h) dT, \quad (3)$$

is symmetric over each orthant comprising BHV treespace. Within each orthant, the integral is equivalent to the normalizing constant of a zero-mean multivariate normal truncated to  $\mathbb{R}_n^+$ . Thus, expression (3) is equivalent to the number of orthants in the space,  $n_O$ , multiplied by the corresponding truncated normal constant.

On the other extreme, consider a central tree  $T'$  such that every edge is large compared to the bandwidth  $h$ , i.e. the tree is relatively far away from any orthant boundary. In this case, the kernel integral will be very close to the value given in expression (2). If the central point is placed arbitrarily far away from any orthant boundary, then the integral over any orthant other than the one containing  $T'$  can be made arbitrarily small. Thus, the integral over the orthant containing  $T'$  itself will be an increasingly good estimate of the entire normalizing constant as the central point is moved further away from orthant boundaries.

The updated version of KDE TREES presented in this paper improves on the first generation algorithm by estimating the kernel normalizing constants  $c(T', h)$ . This is accomplished by finding bounding functions in each orthant which can be more easily integrated than the true kernel function. While some analytic simplification is possible, certain expressions cannot be evaluated other than through numerical methods.

## 1.1 Holonomic Gradient Method

The *holonomic gradient method* (HGM) is a non-stochastic numerical method for calculating certain types of integrals. The HGM is a variation on the gradient descent method of function optimization, and is suitable for application to holonomic functions [Nakayama *et al.*, 2011; Koyama *et al.*, 2014]. Roughly, a holonomic function is a solution to a homogenous ordinary differential equation with polynomial coefficients [Zeilberger, 1990]. Several integrals of interest to statisticians turn out to be expressible as solutions to an optimization problem within a holonomic system.

For our present problem two cases are of particular use. Marumo *et al.* [2014] demonstrates the use of HGM to calculate the normalizing constant for a multivariate normal distribution truncated to the positive orthant, i.e.,  $\mathbb{R}_n^+$ . In addition, Hayakawa and Takemura [2014] provides the constants for the so-called exponential-polynomial family of probability densities,

$$f(x|\theta_1, \dots, \theta_k) \propto \exp\left(x\theta_1 + \dots + x^k\theta_k\right).$$

As was briefly discussed in section 1, BHV treespace is a simplicial complex of positive Euclidean orthants, and the normalizing constant for a truncated multivariate normal distribution is an ingredient for a scheme to approximate the kernel constants in BHV treespace. In section 3 we show that it is possible to use the normalizing constants for the truncated multivariate normal and the exponential-polynomial family, computed either by HGM or some other method, to construct approximations to the kernel normalizing constants for BHV space.

## 2 Methods

### 2.1 Normalizing Constants

In this paper we use  $k$  to denote the *unnormalized* kernel function, i.e., with unit constant of proportionality in (1). If we are given a fixed tree  $T_0$  and bandwidth  $h$ , our objective is to compute bounds for the integral  $K(T_0, h) = \int k(T, T_0, h) dT$  over the entire BHV treespace, so that we may normalize the kernel function.

One suitable lower bound function is based on the use of the triangle inequality.

**Lemma 1.** For any pair of trees,  $k(T, T', h) \geq \underline{k}(T, T', h)$ . Where,

$$\underline{k}(T, T', h) = \exp\left(-\frac{(d(T, 0) + d(0, T'))^2}{h^2}\right).$$

*Proof.* This is an immediate consequence of the fact that the geodesic path between any two trees is the shortest path connecting the trees. In particular, it is shorter than the cone path,  $d(T, T') \leq d(T, 0) + d(0, T')$ .  $\square$

However,  $\underline{k}$  does better than simply providing a global lower bound for  $k$ . In fact, the bound is sharp, as  $\underline{k}$  is equivalent to  $k$  whenever the geodesic between  $T$  and  $T'$  passes through the origin. This turns out to be a quite common occurrence, as geodesics between trees which are not separated by a small number of NNI interchanges are likely to pass through the origin. As a result for much of the space, integrating over  $\underline{k}$  will be equivalent to integrating over  $k$  itself. Happily, integrating  $\underline{k}$  over a single orthant affords an opportunity for analytical simplification.

**Theorem 2.1.** Let  $O$  be an arbitrary fixed orthant in BHV treespace, and let  $p$  denote its dimension. Then, the integral of  $\underline{k}(T, T', h)$  over that orthant is given by the expression

$$\begin{aligned}\underline{C}_O(T', h) &:= \int_O \underline{k}(T, T', h) dT \\ &= \frac{\pi^{p/2} e^{-d(0, T')^2/h^2}}{2^{p-1} \Gamma(p/2)} \underline{A}(T', h).\end{aligned}\tag{4}$$

Where, if we let  $\theta_1 = -2d(0, T')/h^2$  and  $\theta_2 = -h^{-2}$ , then

$$\underline{A}(T', h) = \int_0^\infty r^{p-1} \exp(\theta_1 r + \theta_2 r^2) dr.\tag{5}$$

*Proof.* The distance  $d(T, 0)$  is the usual  $l_2$ -norm of the vector of edge lengths for the tree  $T$ , and  $O$  is the positive orthant  $\mathbb{R}_p^+$ . Thus, if we express the integral over  $O$  in an angular coordinate system,

$$\begin{aligned}\underline{C}_O(T', h) &= e^{-\frac{d(0, T')^2}{h^2}} \int_O e^{-\frac{(d(T, 0)^2 + 2d(0, T')d(T, 0))}{h^2}} dT \\ &= e^{-\frac{d(0, T')^2}{h^2}} \int_0^\infty \int_\Theta e^{\theta_1 r + \theta_2 r^2} dV(r, \Theta)\end{aligned}\tag{6}$$

Now the volume element in  $\mathbb{R}^p$  in an angular coordinate system is

$$dV(r, \Theta) = r^{p-1} dr \prod_{k=1}^{p-1} \sin^{p-k-1}(\theta_k) d\theta_k,$$

and it so happens that one of the definitions of the Beta function yields,

$$\int_0^{\pi/2} \sin^{p-k-1}(\theta) d\theta = \frac{1}{2} B((p-k)/2, 1/2).$$

Integrating in all the radial coordinates yields a product of beta functions which telescopes down to the constant appearing in (4). This reduces the problem to a single integral in the radial coordinate, which is equivalent to  $\underline{A}(T', h)$ .  $\square$

Unfortunately, the function  $\underline{A}(T', h)$  has no general closed form solution. However, there are several methods that we can use to obtain a numerical estimate of this value. The HGM method developed in Hayakawa and Takemura [2014] is one such method for obtaining this value. It is also reasonable to calculate this particular integral using classical quadrature methods.

**Lemma 2.** Following the notation of Hayakawa and Takemura [2014],

$$\underline{A}(T', h) = \partial_1^{p-1} A_2(\theta_1, \theta_2).$$

Here,  $A_2(\theta_1, \theta_2)$  is the normalizing constant for the exponential-polynomial distribution of order 2, the  $\theta$  are defined as in Theorem 2.1, and  $\partial_1^m$  means the  $m$ -th partial derivative with respect to  $\theta_1$ . Furthermore, Hayakawa gives the following equivalence for the first partial derivative

$$\partial_1 A_2(\theta_1, \theta_2) = -\frac{1}{2\theta_2} \{1 + \theta_1 A_2(\theta_1, \theta_2)\},$$

and for the the higher derivatives,  $m \geq 2$ , the partials can be expressed recursively in terms of lower order derivatives,

$$\begin{aligned}\partial_1^m A_2(\theta_1, \theta_2) &= -\frac{1}{2\theta_2} \{(m-1) \partial_1^{m-2} A_2(\theta_1, \theta_2) + \\ &\quad \theta_1 \partial_1^{m-1} A_2(\theta_1, \theta_2)\}.\end{aligned}\tag{7}$$

*Proof.* See Hayakawa and Takemura [2014], Section 2, equations (4) and (7). The latter expression can be easily obtained by differentiation of the expression for the first partial.  $\square$

These results are sufficient to use the *hgm* package described in Koyama *et al.* [2014] to implement the lower bound for the orthant integral,  $\underline{C}_O(T', h)$ .

The desired normalization constant for function (1) can be decomposed as the sum of integrals over each orthant in BHV space. Thus, if  $n_O$  is the number of orthants in the BHV space, then  $n_O \cdot \underline{C}_O(T', h)$  is a crude lower bound for the overall normalizing constant. Although this is a poor bound, it can be improved by obtaining better bounds for the contribution from various orthants and adjusting accordingly.

The most obvious orthant to begin with is the orthant containing the “central” tree  $T'$ , which we shall call  $O_{T'}$ . This is the orthant where the difference between  $k$  and  $\underline{k}$  will be the greatest, and thus the largest improvement to the bounding constant is to be found here. Note that in this case, the integral over  $O_{T'}$  is given by,

$$\begin{aligned} C_{O_{T'}}(T', h) &= \int_{O_{T'}} \exp(d(T', T)^2/h^2) dT \\ &= \int_{\mathbb{R}_p^+} \exp(-\|x - x_{T'}\|/h^2) dx. \end{aligned} \tag{8}$$

This is simply the integral of a radially-symmetric multivariate gaussian kernel centered at the point  $T$  over the positive orthant. Such a normalizing constant can also be calculated using HGM, and an implementation is included in the *hgm* R package [Koyama *et al.*, 2014].

Further improvements to the integral for orthants which adjoin directly to  $O_{T'}$  can be made by noting that a relationship similar to that of Lemma 1 will hold, but with the third point in the triangle inequality being somewhere on the orthant boundary, instead of the origin. However, in practice the improvements to the bounds obtained in this way are quite small, given the typical values of the bandwidths which occur in practice and the small number of orthants to which the calculations apply. For this reason, and in the interests of controlling the overall numerical complexity of the KDETREES algorithm, these “second-order” approximations are not implemented at at this time, but may appear in future updates.

## 2.2 Outlier Test

In Weyenberg *et al.* [2014] we chose to implement a outlier test of the form,  $\hat{f}(T_i) < c^*$ , where the critical value  $c^*$  is selected using Tukey’s quartile method,

$$c^* = Q_1 - k(Q_3 - Q_1).$$

Here,  $\hat{f}(T)$  denotes our density estimate for tree  $T$ , and the quartiles,  $Q_1, Q_3$ , are calculated using all observed tree density estimates.

Further experimentation with the method has suggested that better performance is obtained if the tree density scores are transformed to the log-scale before the classification step takes place,  $\log f(T_i) < c^*$ . This transformation was chosen because the raw scores,  $f(T_i)$ , are themselves bounded below by zero, and the log transformation removes this bound. The quantiles used to compute the critical value are also obtained using the log-transformed scores. Due to the better performance characteristics of this method, the default classifier algorithm for KDETREES has been changed to operate on the log-density scale.

## 2.3 Leaf Edges

The dimension of the orthants comprising tree space is determined by the number of taxa in the trees, with each edge in the fully-resolved tree contributing a dimension to each of the orthants comprising the space. However, the  $n$  leaf edges are represented in the space in such a way that the space can be decomposed into a Cartesian product  $S \times \mathbb{R}_n^+$ . The portion of the space  $S$  is associated with the internal edges of the trees, while the positive euclidean orthants  $\mathbb{R}_n^+$  are associated with the leaf edges [Billera *et al.*, 2001]. Because of this decomposition, there is not a large amount of topological information contained in the portion of the space corresponding to the leaf edge lengths.

If we remove the leaf edges from the calculation, the dimension of treespace can be reduced by approximately half, while retaining the important topological information. This has the benefit of simplifying the overall density estimation problem, as well as the computation of the normalizing constant estimates by the HGM methods. While the original KDETREES algorithm included the leaf edges in the geodesic calculations, the updated version omits them from consideration. A new option flag allows for restoration of the original functionality.

## 3 Results

The updated version of the KDETREES software package is available both from CRAN (the official R package system), as well as from the official development repository on Github. ([github.com/grady/kdetrees](https://github.com/grady/kdetrees)).

### 3.1 Simulations

A set of simulated datasets were constructed and analyzed, using a similar design as the first simulation described in Weyenberg *et al.* [2014]. The simulations measure the true and false positive rates for identification of known outlier trees within a set of trees drawn from a common distribution. Results of the simulation are summarized as ROC curves, and are presented in Figure 1.

### 3.2 Apicomplexa

The Apicomplexa data set presented by Kuo *et al.* [2008] consists of trees reconstructed from 268 single-copy genes from the following species: *Babesia bovis* (Bb) [Brayton *et al.*, 2007] (GenBank accession numbers AAXT01000001–AAXT01000013), *Cryptosporidium parvum* (Cp) [Abrahamsen *et al.*, 2004] from CryptoDB.org [Heiges *et al.*, 2006], *Eimeria tenella* (Et) from GeneDB.org [Hertz-Fowler *et al.*, 2004], *Plasmodium falciparum* (Pf) [Gardner *et al.*, 2002] and *Plasmodium vivax* (Pv) from PlasmoDB.org [Bahl *et al.*, 2003], *Theileria annulata* (Ta) [Pain *et al.*, 2005] from GeneDB.org [Hertz-Fowler *et al.*, 2004], and *Toxoplasma gondii* (Tg) from Toxo-DB.org [Gajria *et al.*, 2008]. A free-living ciliate, *Tetrahymena thermophila* (Tt) [Eisen *et al.*, 2006], was used as the outgroup. To this set of sequences, we appended the Set8 gene, which has been identified by Kishore *et al.* [2013] as a probable case of horizontal gene transfer from a higher eukaryote to an ancestor of the Apicomplexa. This is the same data set analyzed as part of the original KDETREES paper, which was analyzed again with the updated algorithm. The new set of outlier trees is presented in Table 1. The newly identified set of outlier trees are presented in a series of figures at the end of this manuscript. The figures are in ascending order by the kdetrees tree score, i.e., the first tree depicted is the furthest outlying tree.

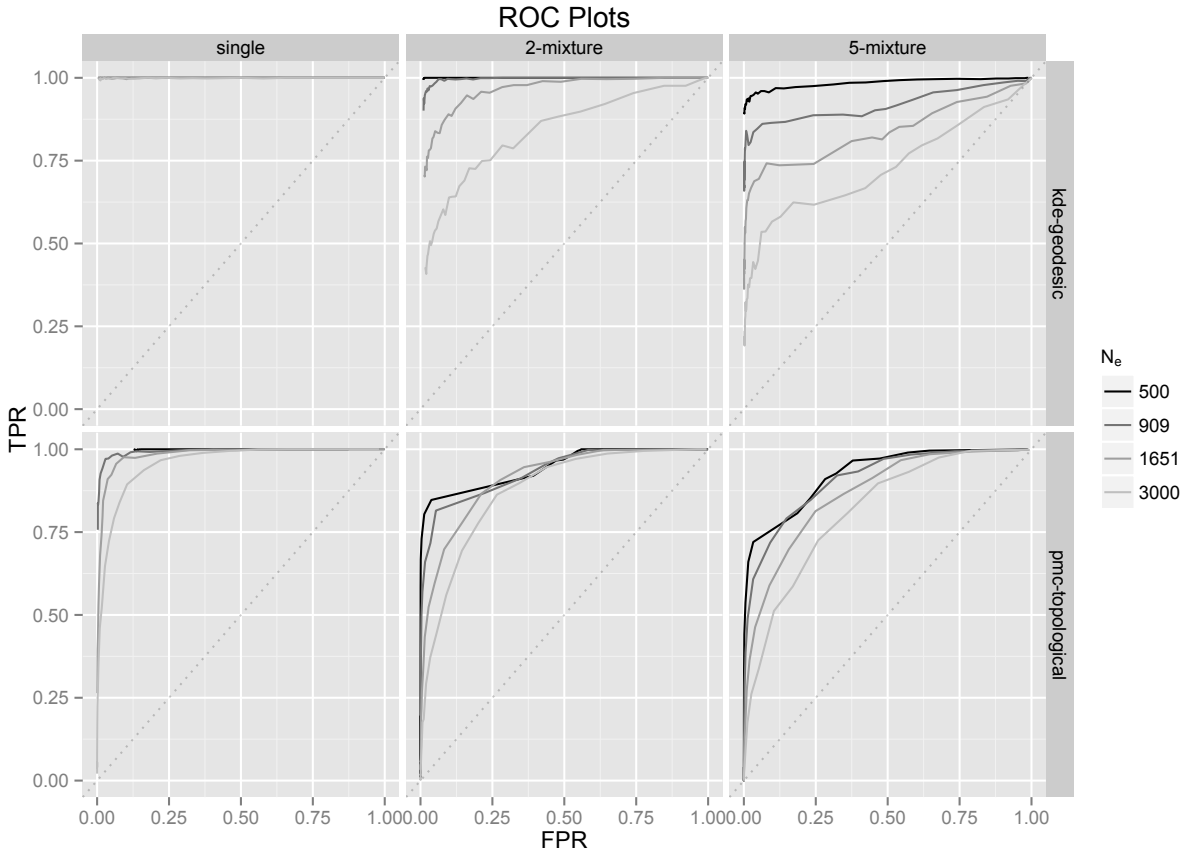


Figure 1: Receiver operating characteristic (ROC) plots comparing the updated KDETREES algorithm with Phylo-MCOA. ROC plots summarize the true and false positive rates for a binary classifier as the tuning parameters are changed. A perfect classifier would be represented as a single point at the upper left corner of the plot, while a completely random scheme would follow the dotted diagonal lines. Curves are shown from simulated coalescent data, using a variety of effective population sizes ( $N_e$ ). Larger values for  $N_e$  correspond to more variability in the generated trees, and thus a more difficult classification problem.

Table 1: Apicomplexa gene sets identified as outliers by the updated KDETREES. Genes which were not identified as outliers by the original algorithm are marked with a \*.

No. <sup>a</sup>	GeneID <sup>b</sup>	Functional Annotation	Analysis
* 472	PF14_0059	hypothetical protein	Tree topology inconsistent with phylogeny. Bb and Cp on same branch, with Ta distant from sister species Bb. Sequence alignment looks good in some regions, but with numerous gaps and other regions with poor alignment. Multiple homopolymer stretches in Pv and Pf.
* 478	PF14_0326	hypothetical protein	Tree topology not consistent with phylogeny of the species. Bb branches with the outgroup Tt instead of its closely-related sister species Ta. Poor alignment with numerous gaps, numerous homopolymer stretches, particularly in Et.
488	PF08_0086	RNA-binding protein, putative	Significant sequence length disparity (164 a.a. for Ta vs 1075a.a. for Pf). Generally good sequence alignment in one region of 100 residues; otherwise, alignment is poor.
* 505	PF14_0143	protein kinase, putative	Ta/Bb and Pf/Pv not monophyletic; split by outgroup Tt. Good sequence alignment in multiple blocks, but significant sequence length differences. Pf/Pv have multiple insertions and Et and Cp sequences are truncated.
515	PFA0390w	DNA repair exonuclease, putative	Short sequences for Et and Cp. Several homopolymer stretches in Et. Modest to good alignment in multiple blocks, Et being an exception in several regions. Possible incorrect annotation of Et sequence.
* 553	PFC0730w	conserved protein, putative	Tree topology inconsistent with phylogeny. Bb and Ta are distant not monophyletic with Pv/Pf. Short regions exhibiting good sequence alignment. Et sequence is truncated.
* 578	PF14_0042	U3 small nucleolar ribonucleoprotein, U3 snoRNP putative	Tree topology very inconsistent with phylogeny; Tg branch with outgroup Tt, Et branch with Bb and Ta. Poor alignment. Significant sequence length differences; Tg sequence is 4126 residues in length, Cp and Tt 2000 residues, Pf and Pv are 450 residues.
* 585	PF10_0054	hypothetical protein	Cp exhibits anomalous placement in tree. Significant sequence length differences; Pf, Pv, Tg about 1100 residues, Et only 349 residues, so numerous gaps in alignment. Some regions show good alignment.
* 588	PFI1020c	Inosine-5'-monophosphate dehydrogenase	Sequence alignment looks reasonably good. Tree shows Cp branching with outgroup Tt and distant from other Api species. Bb split from Ta.
* 630	PFL2120w	hypothetical protein, conserved	Tree topology inconsistent with phylogeny. Cp branching with Pv/Pf. Ta/Bb not monophyletic with Pv/Pf. Several blocks of sequence showing good alignment, but numerous gaps, due mostly to Ta insertions.
641	PFE0750c	hypothetical protein, conserved	Et on a very long branch with other species tightly clustered. Large difference in sequence lengths; 269 residues for Et vs. 848 for Pf. Central region with modest to good alignment; Et exhibited poor sequence identity.
* 645	PF14_0635	RNA binding protein, putative	Tree topology looks proper, although Pv and Pf are on a somewhat long branch. Modest to good alignment.
* 662	PF11_0463	coat protein, gamma subunit, putative	Multiple homopolymer stretches in Et sequence. Generally good alignment for all but Et; sequence might not be homologous.
* 725	PF14_0428	histidine - tRNA ligase	Tree topology appears proper, but Pf/Pv on long branch. Good alignment in two large blocks, but significant gaps and poor alignment in other regions. Et sequence truncated (339 vs. 1000 residues for others). Ta sequence also truncated (583 residues).
* 745	PF11_0049	hypothetical protein, conserved	Ta and Bb branch is distant from other Api species, which cluster tightly. Regions of good sequence alignment by with several large gaps. Sequence length differences; Pf and Pv = 3300 residues, Tg and Cp = 2600, Et only 347.
* 750	PFE1050w	adenosylhomocysteinase (S-adenosyl-L-homocysteine hydrolase)	Ta and Bb somewhat distant from other Api species. Relatively good sequence alignment, although Et sequence truncated (291 vs. 480 for others).

<sup>a</sup>Based on geneset designations in Kuo *et al.* [2008].

<sup>b</sup>Geneset represented by GeneID for *Plasmodium falciparum*.

Pf = *Plasmodium falciparum*, Pv = *Plasmodium vivax*, Pb = *Bebaesia bovis*, Ta = *Theileria*

## 4 Discussion

### 4.1 Apicomplexa

The outliers identified by `KDETTREES` in the Apicomplexa dataset are substantially different than those reported in our original paper. In the original paper, many of the outliers were trees containing a single edge much longer than any other edge. This was largely attributable to one or more poorly aligned sequences within the larger multiple sequence alignment. Thus, the disproportionate edges were often leaf edges, and as a result of the changes in the algorithm, the leaf edges are no longer taken into consideration by the default settings. As a result, many of the trees identified as outliers in the original paper are no longer identified as outliers by the default parameter settings of the improved version. Of course, there is a new option flag available, which can be used to restore the behavior found in the original paper. The software also retains the “dissimilarity mode” from the original implementation, which always uses the terminal branch length information.

The cumulative result of the changes in the algorithm is an increased focus on differences in topology in the dataset. The new set of 16 outlying trees differ from the non-outliers primarily in the placement of the Bb, Cp, Ta, and Tt genes within the trees. In the non-outlier trees, Cp generally forms a clade with Tt, while Ta forms a clade with Bb. In the outlier trees, however, these taxa are placed in widely varying locations within the trees, as demonstrated by the tree drawings of outlier trees found at the end of this manuscript.

Together, these results demonstrate that the updated `KDETTREES` algorithm is more sensitive to topological differences in the trees than the previous version, at the expense of the loss of information from the terminal edge lengths. However, the original functionality using the terminal edge information is still available for use, by setting the appropriate flags.

### 4.2 Simulations

The performance of the classifier with the simulated datasets is substantially better than the original version of the algorithm. Although there is a modest performance penalty associated with the estimation of the normalizing constants, `kdetrees` remains significantly faster than the competitor `Phylo-MCOA` algorithm [de Vienne *et al.*, 2012].

When the non-outlier trees are drawn from a single coalescent distribution, the performance of the classifier is nearly perfect, identifying the correct outlier in every simulation iteration, even when the variance of the coalescent distributions (controlled by the effective population size parameter  $N_e$ ) was quite large. (Of course, due to the nature of the classifier, false positives are inevitable if the tuning parameter is chosen poorly.) In the more difficult cases where the non-outliers were drawn from a mixture of coalescent distributions, the updated algorithm remained superior to the `Phylo-MCOA` algorithm, showing greater area under the ROC curve for all cases except for the case of the most highly variable 5-part mixture distribution for the non-outlier trees.

## 5 Conclusion

Our proposed method is motivated by the fact that existing methods of phylogenetic analysis and tree comparisons are not adequate for genomic scale phylogenetic analysis, particularly in cases of certain non-canonical evolutionary phenomena. Furthermore, the scenario in our mixed coalescent distribution simulation—where the non-outlier trees are sampled from an unknown mixture of distributions—cannot be handled by parametric methods, with the possible exception of the genome spectral methods. However, even the genome spectral methods ignore possible statistical

dependencies between different feature spectra. In contrast, we propose analyzing a collection of gene trees without reducing gene trees to summarizing information. Our **kdetrees** approach also possesses a considerable advantage in speed over other methods, which is of paramount importance for a tool used in whole-genome phylogenetic analysis.

In addition, one of the applications of our method is an inference on the species tree or a tree that reflects the evolution of most genes in the genome. We can use our method to identify genes which produce discordant trees (outlying trees) and then we can remove them from phylogenetic analysis. By doing this we can use the genes that share the same evolutionary history and we can build a tree that reflects the evolution of the species or that of most of the genome.

We have been interested in developing a phylogenomic pipeline that is convenient and accessible, as well as robust. To accomplish this aim, an important problem that needs attention is to comparing thousands of gene phylogenies across whole genomes. Thus, our approach is focused on the efficiency of the algorithm in terms of computational complexity and memory requirements, with less emphasis on achieving the highest classification accuracy possible. Thus, it is very important for us to improve the accuracy of the method while we maintain the speed of the algorithm. Compared with the original **kdetrees** and the Phylo-MCOA algorithm, in this paper, we have demonstrated the significant improvement in the accuracy of the method without costing the computational speed (see the simulation results in Figure 1).

In future work we intend to apply **kdetrees** to clustering trees based on similarity. Unsupervised clustering is an important method to learn the structure of unlabeled data. The aim of clustering methods is to group patterns on the basis of a similarity (or dissimilarity) criteria where groups (or clusters) are set of similar patterns.

Many traditional clustering algorithms (e.g., K-Means, Fuzzy c-Means, SOM and Neural Gas) have the version of kernel-based algorithms [Hur *et al.*, 2000, 2001; Camastra and Verri, 2005]. The use of kernels allows to map implicitly data into an high dimensional space, called feature space; computing a linear partitioning in this feature space results in a nonlinear separation between clusters in the input space. Using kernels defined in the space of trees, mapped into vector spaces, to evaluate trees' structural similarity allows us to use Kernel-based clustering methods to group trees in the space.

## References

- Mitchell S. Abrahamsen, Thomas J. Templeton, Shinichiro Enomoto, Juan E. Abrahante, Guan Zhu, Cheryl A. Lancto, Mingqi Deng, Chang Liu, Giovanni Widmer, Saul Tzipori, Gregory A. Buck, Ping Xu, Alan T. Bankier, Paul H. Dear, Bernard A. Konfortov, Helen F. Spriggs, Lakshminarayan Iyer, Vivek Anantharaman, L. Aravind, and Vivek Kapur. Complete genome sequence of the apicomplexan, *cryptosporidium parvum*. *Science*, 304:441–445, 2004.
- Amit Bahl, Brian Brunk, Jonathan Crabtree, Martin J. Fraunholz, Bindu Gajria, Gregory R. Grant, Hagai Ginsburg, Dinesh Gupta, Jessica C. Kissinger, Philip Labo, Li Li, Matthew D. Mailman, Arthur J. Milgram, David S. Pearson, David S. Roos, Jonathan Schug, Christian J. Stoeckert, and Patricia Whetzel. Plasmodb: the plasmodium genome resource. a database integrating experimental and computational data. *Nucleic Acids Res.*, 31:212–215, 2003.
- L.J. Billera, S.P. Holmes, and K. Vogtmann. Geometry of the space of phylogenetic trees. *Adv Appl Math*, 27(4):733–767, 2001.
- Kelly A. Brayton, Audrey O. T. Lau, David R. Herndon, Linda Hannick, Lowell S. Kappmeyer, Shawn J. Berens, Shelby L. Bidwell, Wendy C. Brown, Jonathan Crabtree, Doug Fadrosh,

- Tamara Feldblum, Heather A. Forberger, Brian J. Haas, Jeanne M. Howell, Hoda Khouri, Hean Koo, David J. Mann, Junzo Norimine, Ian T. Paulsen, Diana Radune, Qinghu Ren, Roger K. Smith Jr., Carlos E. Suarez, Owen White, Jennifer R. Wortman, Donald P. Knowles Jr.1, Terry F. McElwain, and Vishvanath M. Nene. Genome sequence of babesia bovis and comparative analysis of apicomplexan hemoprotezoa. *PLoS Pathog*, 3:e148, 2007.
- F. Camastra and A. Verri. A novel kernel method for clustering. *IEEE Transactions on Pattern Analysis and Machine Intelligence*, 27(5):801–804, 2005.
- D. M. de Vienne, S. Ollier, and G. Aguileta. Phylo-mcoa: A fast and efficient method to detect outlier genes and species in phylogenomics using multiple co-inertia analysis. *Mol Biol Evol*, 2012.
- Jonathan A Eisen, Robert S Coyne, Martin Wu, Dongying Wu, Mathangi Thiagarajan, Jennifer R Wortman, Jonathan H Badger, Qinghu Ren, Paolo Amedeo, Kristie M Jones, Luke J Tallon, Arthur L Delcher, Steven L Salzberg, Joana C Silva, Brian J Haas, William H Majoros, Maryam Farzad, Jane M Carlton, Roger K Smith, Jr., Jyoti Garg, Ronald E Pearlman, Kathleen M Karrer, Lei Sun, Gerard Manning, Nels C Elde, Aaron P Turkewitz, David J Asai, David E Wilkes, Yufeng Wang, Hong Cai, Kathleen Collins, B. Andrew Stewart, Suzanne R Lee, Katarzyna Wilamowska, Zasha Weinberg, Walter L Ruzzo, Dorota Wloga, Jacek Gaertig, Joseph Frankel, Che-Chia Tsao, Martin A Gorovsky, Patrick J Keeling, Ross F Waller, Nicola J Patron, J. Michael Cherry, Nicholas A Stover, Cynthia J Krieger, Christina del Toro, Hilary F Ryder, Sondra C Williamson, Rebecca A Barbeau, Eileen P Hamilton, and Eduardo Orias. Macronuclear genome sequence of the ciliate *Tetrahymena thermophila*, a model eukaryote. *PLoS Biol.*, 4:1620–1642, 2006.
- Bindu Gajria, Amit Bahl, John Brestelli, Jennifer Dommer, Steve Fischer, Xin Gao, Mark Heiges, John Iodice, Jessica C. Kissinger, Aaron J. Mackey, Deborah F. Pinney, David S. Roos, Christian J. Stoeckert, Haiming Wang, and Brian P. Brunk. Toxodb: an integrated toxoplasma gondii database resource. *Nucleic Acids Res.*, 36:D553–D556, 2008.
- Malcolm J. Gardner, Neil Hall, Eula Fung, Owen White, Matthew Berriman, Richard W. Hyman, Jane M. Carlton, Arnab Pain, Karen E. Nelson, Sharen Bowman, Ian T. Paulsen, Keith James, Jonathan A. Eisen, Kim Rutherford, Steven L. Salzberg, Alister Craig, Sue Kyes, Man-Suen Chan, Vishvanath Nene, Shamira J. Shallom, Bernard Suh, Jeremy Peterson, Sam Angiuoli, Mihaela Pertea, Jonathan Allen, Jeremy Selengut, Daniel Haft, Michael W. Mather, Akhil B. Vaidya, David M. A. Martin, Alan H. Fairlamb, Martin J. Fraunholz, David S. Roos, Stuart A. Ralph, Geoffrey I. McFadden, Leda M. Cummings, G. Mani Subramanian, Chris Mungall, J. Craig Venter, Daniel J. Carucci, Stephen L. Hoffman, Chris Newbold, Ronald W. Davis, Claire M. Fraser, and Bart Barrell. Genome sequence of the human malaria parasite plasmodium falciparum. *Nature*, 419:498–511, 2002.
- Jumpei Hayakawa and Akimichi Takemura. Estimation of exponential-polynomial distribution by holonomic gradient descent, 2014.
- Mark Heiges, Haiming Wang, Edward Robinson, Cristina Aurrecochea, Xin Gao, Nivedita Kaluskar, Philippa Rhodes, Sammy Wang, Cong-Zhou He, Yanqi Su, John Miller, Eileen Kraemer, and Jessica C. Kissinger. Cryptodb: a cryptosporidium bioinformatics resource update. *Nucleic Acids Res.*, 34:D419–D422, 2006.
- Christiane Hertz-Fowler, Chris S. Peacock, Valerie Wood, Martin Aslett, Arnaud Kerhornou, Paul Mooney, Adrian Tivey, Matthew Berriman, Neil Hall, Kim Rutherford, Julian Parkhill, Alas-

- dair C. Ivens, Marie-Adele Rajandream, and Bart Barrell. Genedb: a resource for prokaryotic and eukaryotic organisms. *Nucleic Acids Res.*, 32:D339–D343, 2004.
- A. B. Hur, D. Horn, H. T. Siegelmann, and V. Vapnik. A support vector method for clustering. *NIPS*, pages 367–373, 2000.
- A. B. Hur, D. Horn, H. T. Siegelmann, and V. Vapnik. Support vector clustering. *JMLR*, 2:125–137, 2001.
- S. P. Kishore, J. W. Stiller, and K. W. Deitsch. Horizontal gene transfer of epigenetic machinery and evolution of parasitism in the malaria parasite plasmodium falciparum and other apicomplexans. *Evol Biol*, pages 13–37, 2013.
- Tamio Koyama, Hiromasa Nakayama, Katsuyoshi Ohara, Tomonari Sei, and Nobuki Takayama. Software packages for holonomic gradient method. In *Mathematical Software–ICMS 2014*, pages 706–712. Springer, 2014.
- C. Kuo, J. P. Wares, and J. C. Kissinger. The apicomplexan whole-genome phylogeny: An analysis of incongruence among gene trees. *Mol Biol Evol*, 25(12):2689–2698, 2008.
- Naoki Marumo, Toshinori Oaku, and Akimichi Takemura. Properties of powers of functions satisfying second-order linear differential equations with applications to statistics, 2014.
- Hiromasa Nakayama, Kenta Nishiyama, Masayuki Noro, Katsuyoshi Ohara, Tomonari Sei, Nobuki Takayama, and Akimichi Takemura. Holonomic gradient descent and its application to the fisher-bingham integral. *Advances in Applied Mathematics*, 47(3):639 – 658, 2011.
- M. Owen and J. S. Provan. A fast algorithm for computing geodesic distances in tree space. *IEEE ACM T COMPUT BI*, 8(1):2–13, 2011.
- A. Pain, H. Renauld, and et al. Genome of the host-cell transforming parasite theileria annulata compared with t. parva. *Science*, 309:131–133, 2005.
- G. Weyenberg, P. Huggins, C. Schardl, D.K. Howe, and R. Yoshida. kdetrees: Nonparametric estimation of phylogenetic tree distributions. *Bioinformatics*, 2014.
- Doron Zeilberger. A holonomic systems approach to special functions identities. *Journal of Computational and Applied Mathematics*, 32(3):321 – 368, 1990.

**488.tre**

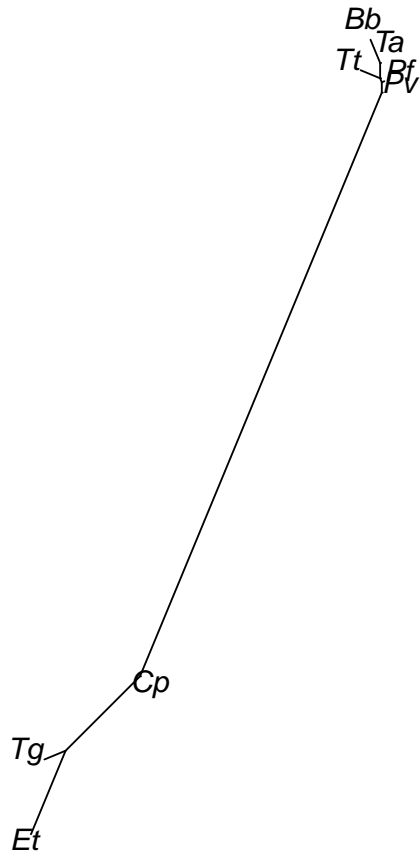


Figure 2: A newly identified outlier from the Apicomplexa dataset.

**478.tre**

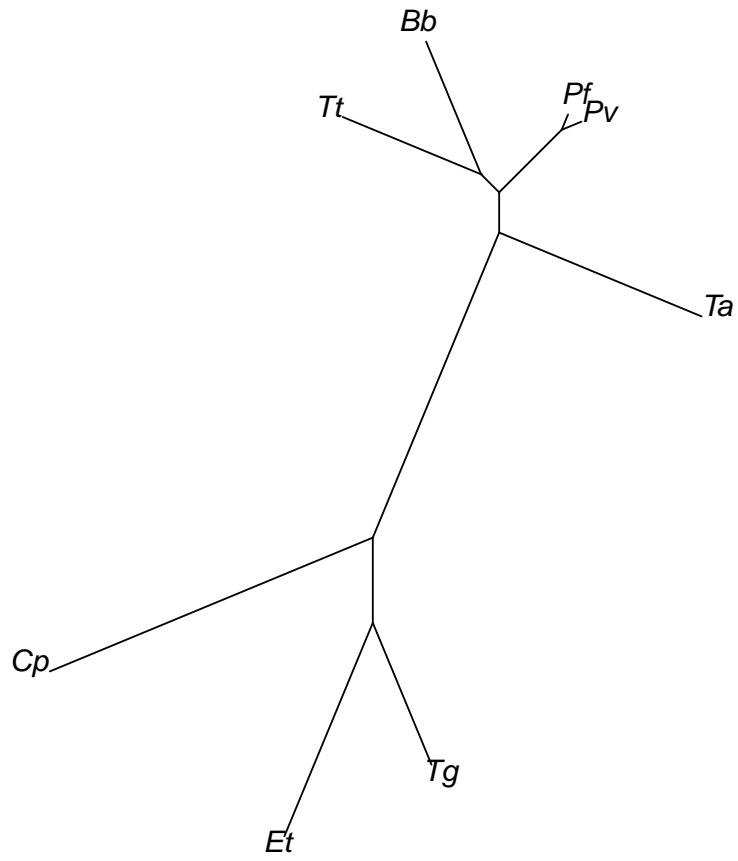


Figure 3: A newly identified outlier from the Apicomplexa dataset.

**515.tre**

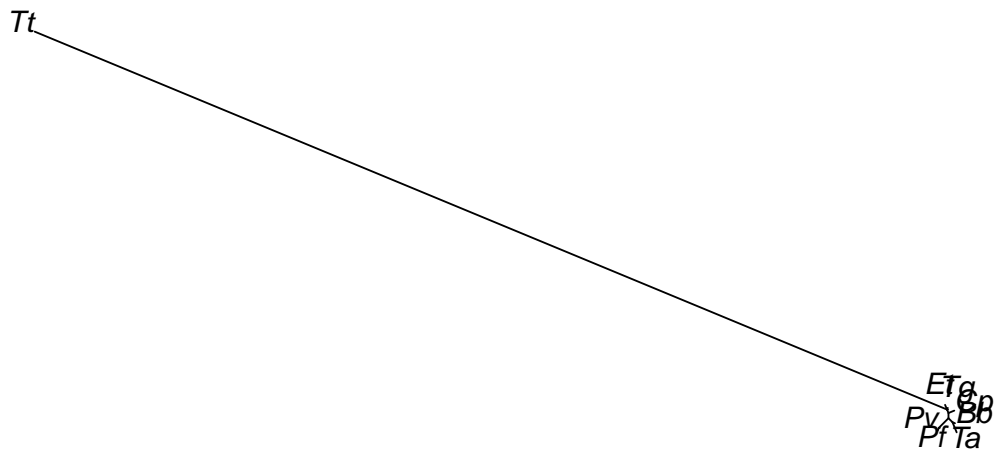


Figure 4: A newly identified outlier from the Apicomplexa dataset.

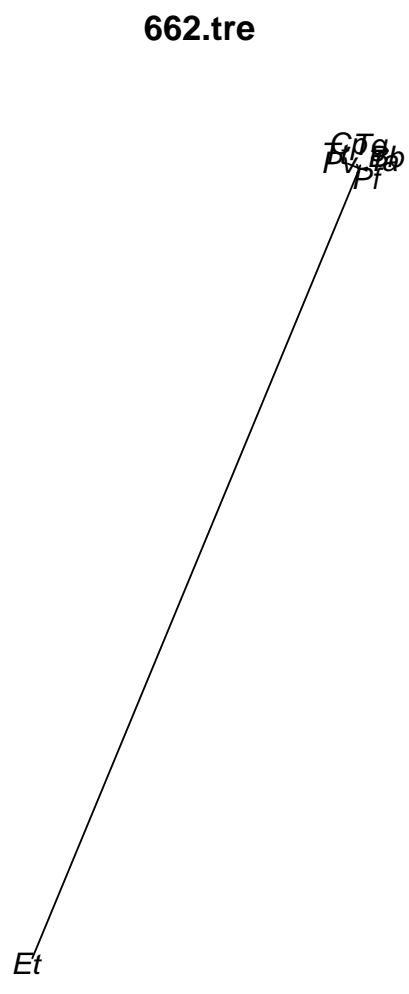


Figure 5: A newly identified outlier from the Apicomplexa dataset.

578.tre

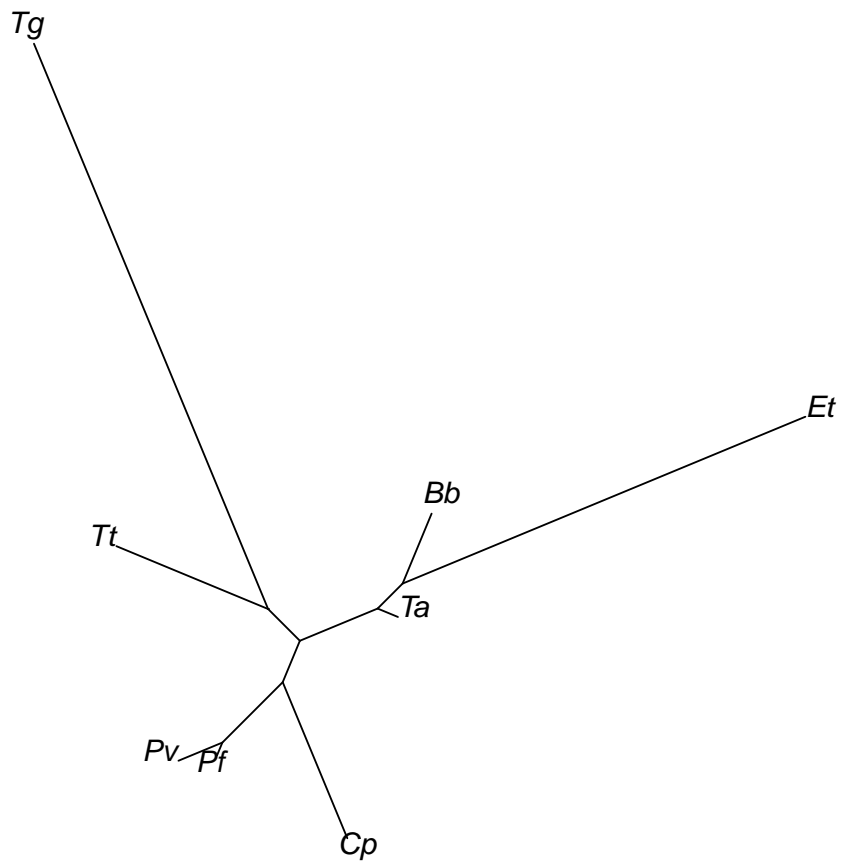


Figure 6: A newly identified outlier from the Apicomplexa dataset.

**588.tre**

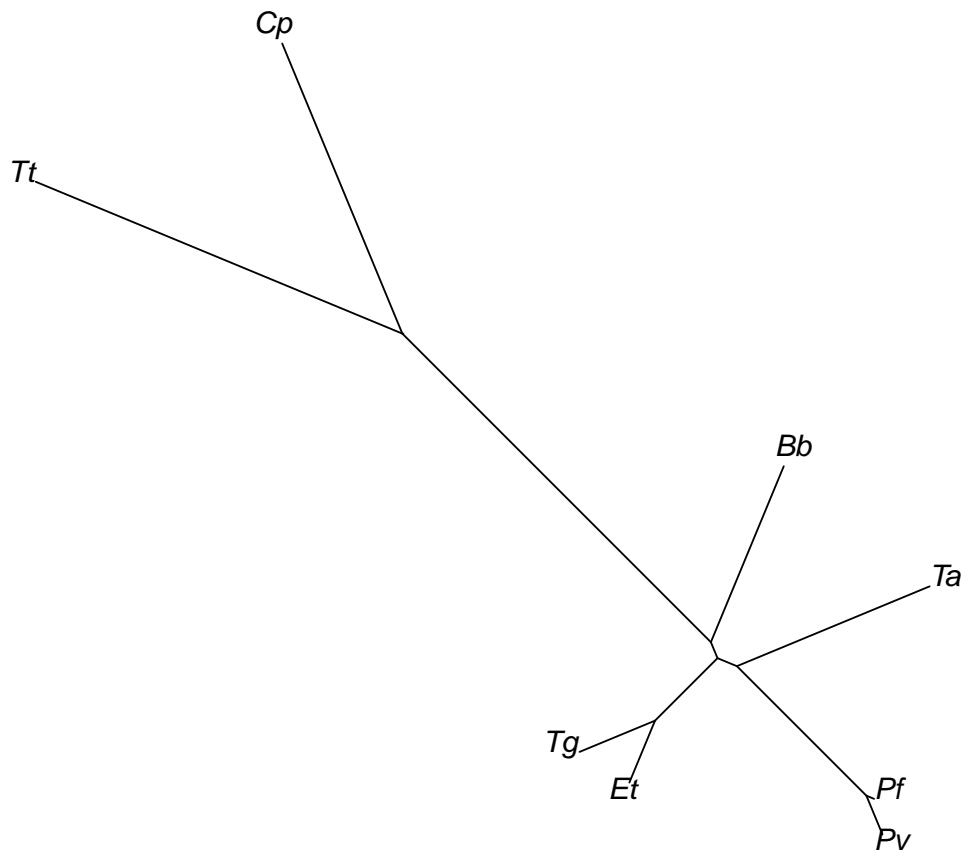


Figure 7: A newly identified outlier from the Apicomplexa dataset.

472.tre

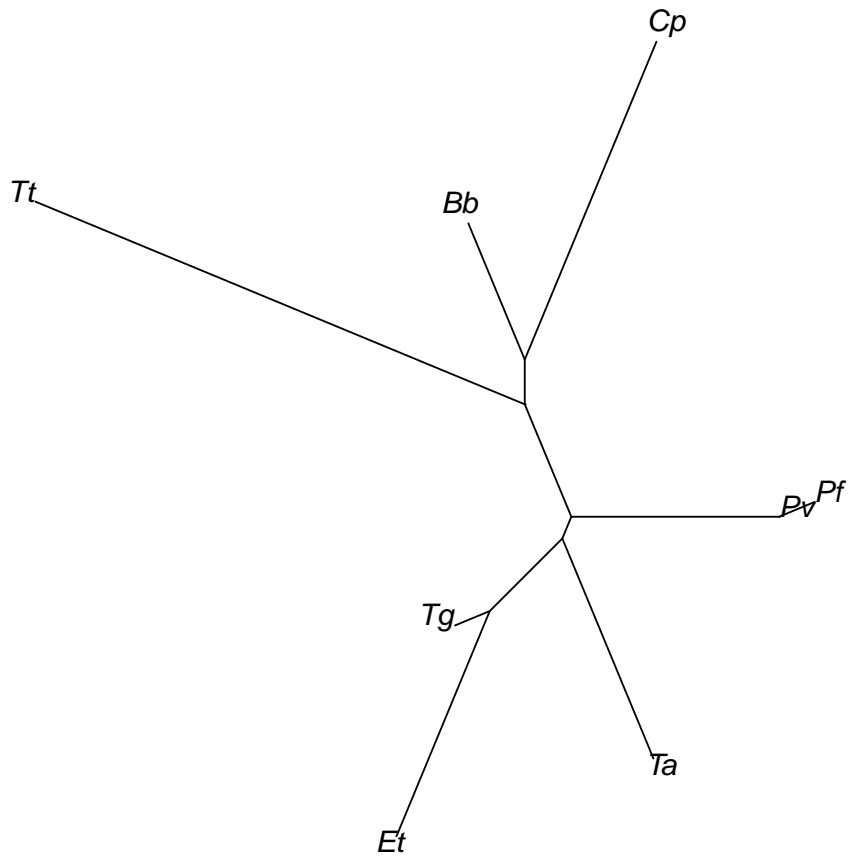


Figure 8: A newly identified outlier from the Apicomplexa dataset.

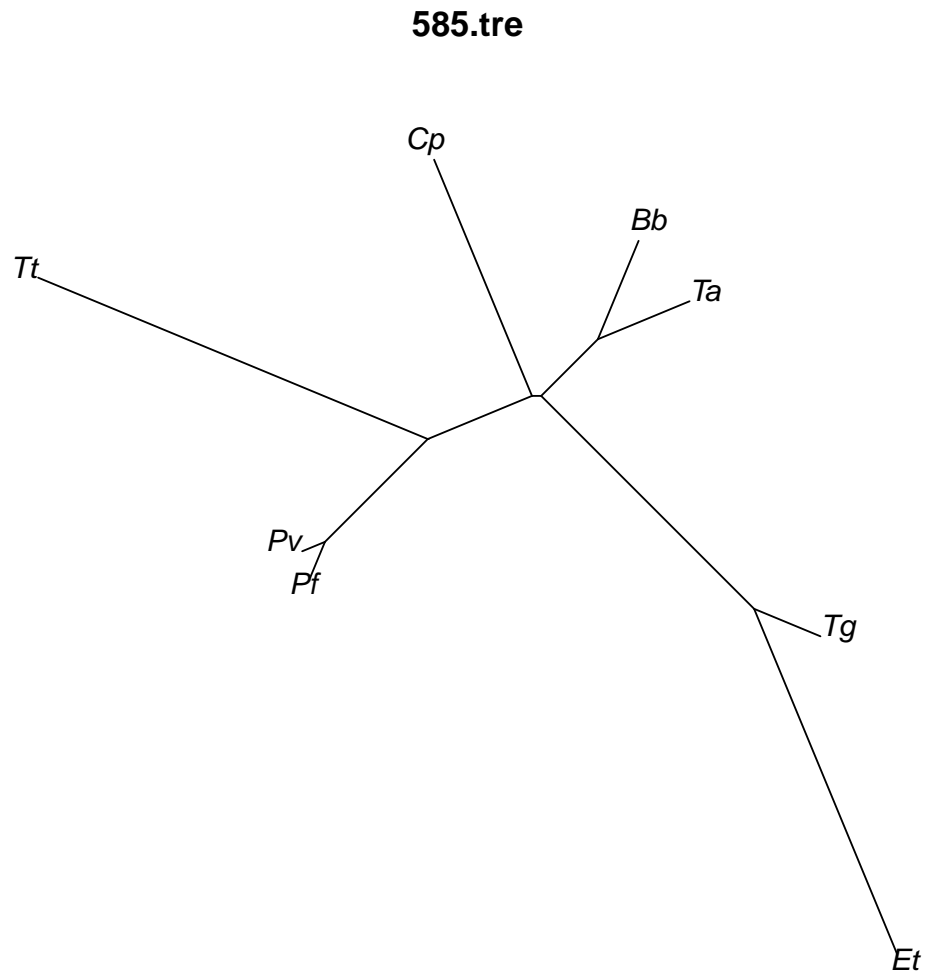


Figure 9: A newly identified outlier from the Apicomplexa dataset.

**745.tre**

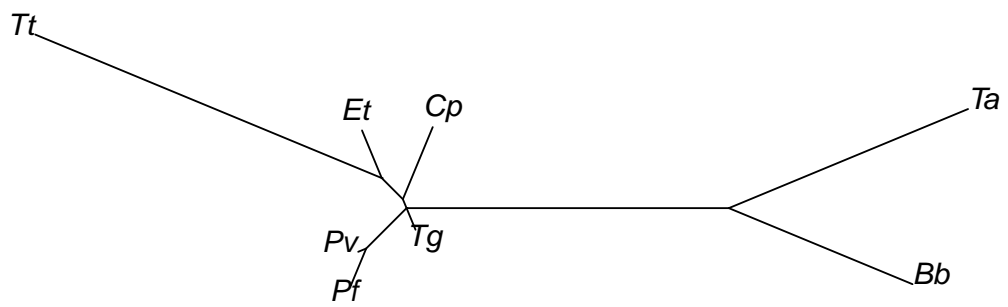


Figure 10: A newly identified outlier from the Apicomplexa dataset.

641.tre

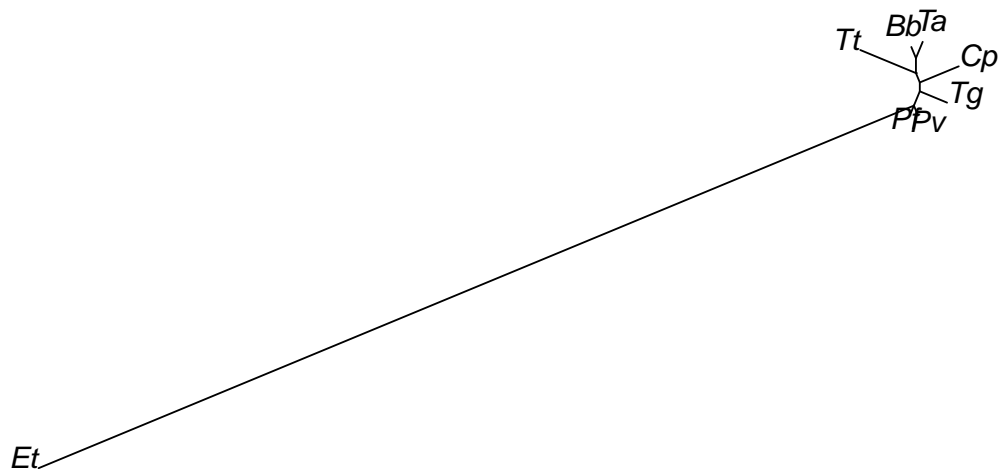


Figure 11: A newly identified outlier from the Apicomplexa dataset.

645.tre

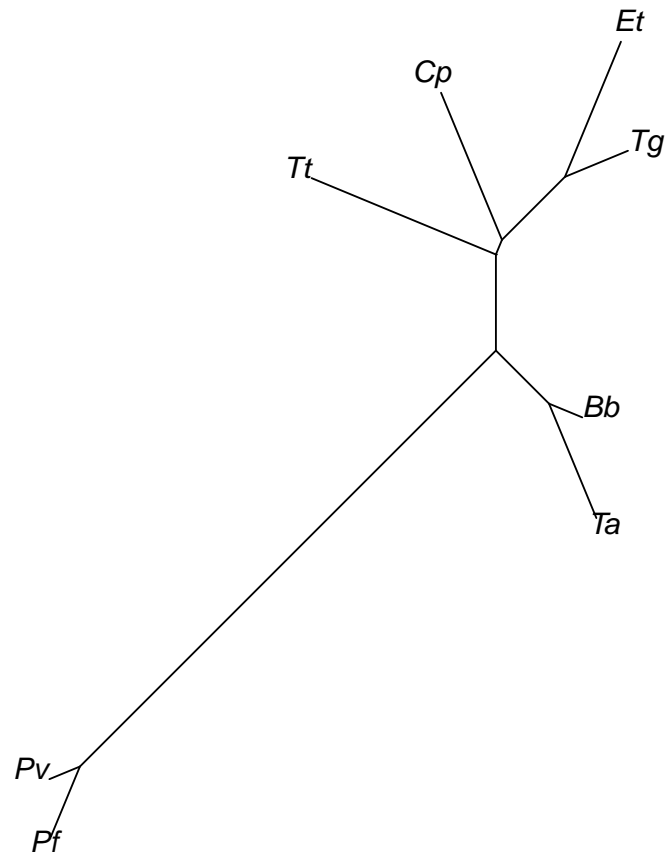


Figure 12: A newly identified outlier from the Apicomplexa dataset.

**750.tre**

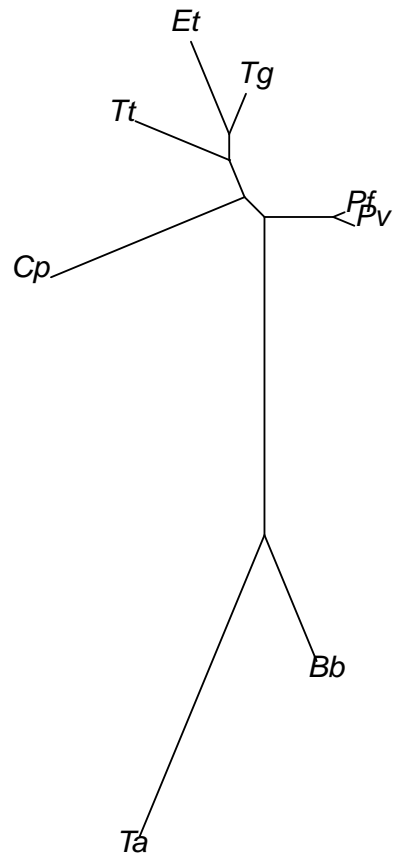


Figure 13: A newly identified outlier from the Apicomplexa dataset.

**553.tre**

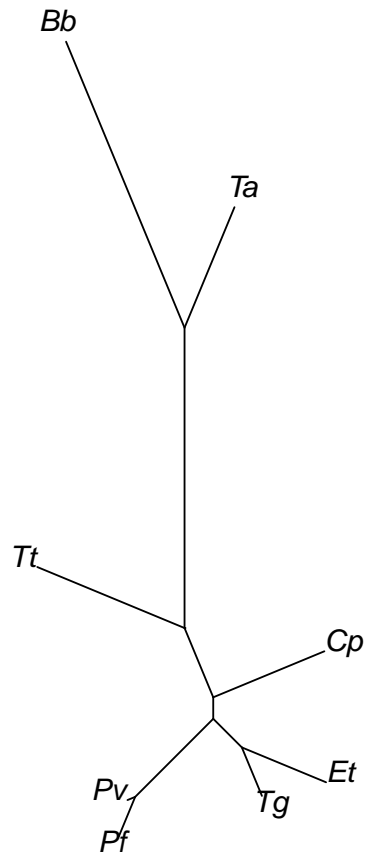


Figure 14: A newly identified outlier from the Apicomplexa dataset.

**630.tre**

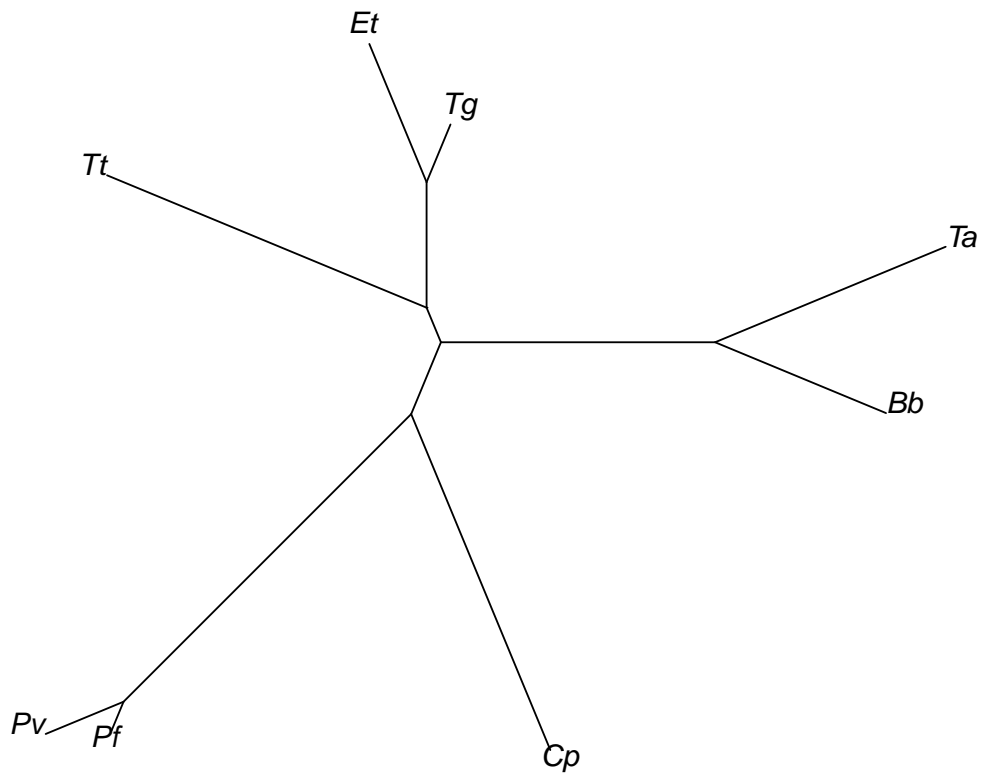


Figure 15: A newly identified outlier from the Apicomplexa dataset.

725.tre

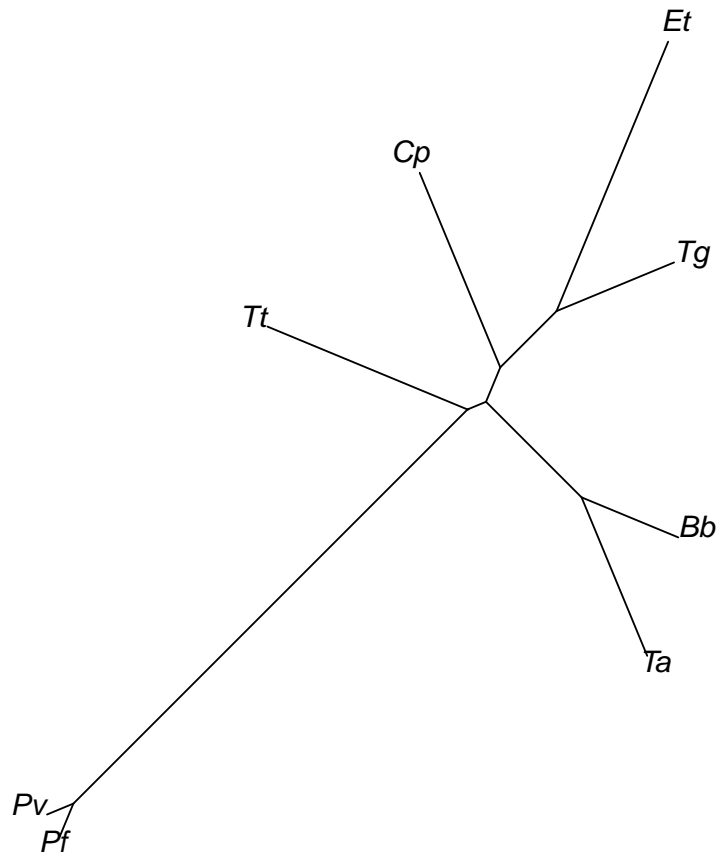


Figure 16: A newly identified outlier from the Apicomplexa dataset.

**505.tre**

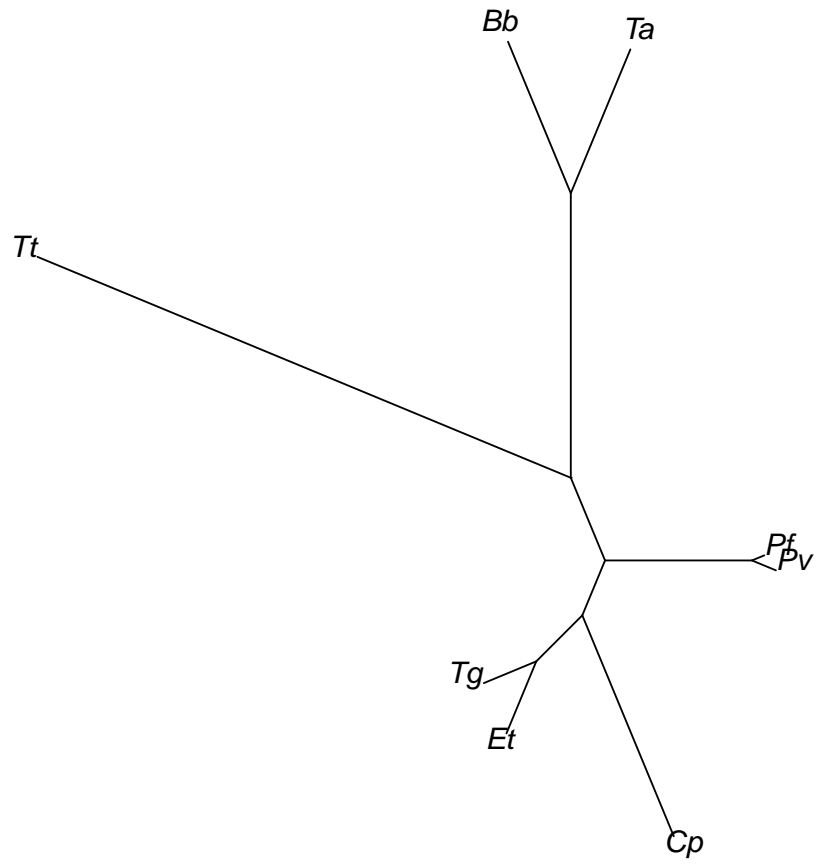


Figure 17: A newly identified outlier from the Apicomplexa dataset.